Kinetics and mechanistic analysis of an extremely rapid carbon dioxide fixation reaction

Deguang Huang[a], Olga V. Makhlynets[b], Lay Ling Tan[c], Sonny C. Lee[c], Elena V. Rybak-Akimova[b], and R. H. Holm[a,1]

[a]Department of Chemistry and Chemical Biology, Harvard University, Cambridge, MA 02138; [b]Department of Chemistry, Tufts University, Medford, MA 02155; and [c]Department of Chemistry, University of Waterloo, Waterloo, ON, Canada N2L3G1

Contributed by R. H. Holm, November 23, 2010 (sent for review October 30, 2010)

Carbon dioxide may react with free or metal-bound hydroxide to afford products containing bicarbonate or carbonate, often captured as ligands bridging two or three metal sites. We report the kinetics and probable mechanism of an extremely rapid fixation reaction mediated by a planar nickel complex $[Ni^{II}(NNN)(OH)]^{1-}$ containing a tridentate 2,6-pyridinedicarboxamidate pincer ligand and a terminal hydroxide ligand. The minimal generalized reaction is M-OH + CO_2 → M-OCO_2H; with variant M, previous rate constants are $\lesssim 10^3$ M^{-1} s^{-1} in aqueous solution. For the present bimolecular reaction, the (extrapolated) rate constant is 9.5×10^5 M^{-1} s^{-1} in N, N′-dimethylformamide at 298 K, a value within the range of $k_{cat}/K_M \approx 10^5$–10^8 M^{-1} s^{-1} for carbonic anhydrase, the most efficient catalyst of CO_2 fixation reactions. The enthalpy profile of the fixation reaction was calculated by density functional theory. The initial event is the formation of a weak precursor complex between the Ni-OH group and CO_2, followed by insertion of a CO_2 oxygen atom into the Ni-OH bond to generate a four center Ni(η^2-OCO_2H) transition state similar to that at the zinc site in carbonic anhydrase. Thereafter, the Ni-OH bond detaches to afford the Ni(η^1-OCO_2H) fragment, after which the molecule passes through a second, lower energy transition state as the bicarbonate ligand rearranges to a conformation very similar to that in the crystalline product. Theoretical values of metric parameters and activation enthalpy are in good agreement with experimental values [$\Delta H^{\ddagger} = 3.2(5)$ kcal/mol].

nickel hydroxide | carbon dioxide–bicarbonate conversion | reaction mechanism

Recent research in this laboratory has been directed toward the attainment of synthetic analogues of the $NiFe_3S_4$ active site of the enzyme carbon monoxide dehydrogenase (1, 2), which catalyzes the interconversion reaction $CO_2 + 2H^+ + 2e^- \rightleftharpoons CO + H_2O$. In the course of this work, we have prepared binuclear Ni^{II}/Fe^{II} bridged species with the intention of simulating the Ni…Fe component of the enzyme site that is the locus of substrate binding, activation, and product release (3). The nickel site in the binuclear species has been prepared separately in the form of the planar hydroxide complex $[Ni(pyN_2^{Me2})(OH)]^{1-}$ containing a N,N′-2,6-dimethylphenyl-2,6-pyridinedicarboxamidate dianion. Whereas bridging hydroxide ligation is common, terminal binding is not and in general is stabilized in divalent metal complexes by hydrogen bonding or by steric shielding, as is the case here. As reported recently (3), exposure of a solution of $[Ni(pyN_2^{Me2})(OH)]^{1-}$ to the atmosphere results in an instantaneous color change from red to red–orange. This results in the fixation of CO_2 as the bicarbonate complex $[Ni(pyN_2^{Me2})(HCO_3)]^{1-}$ accompanied by the spectral changes in Fig. 1.

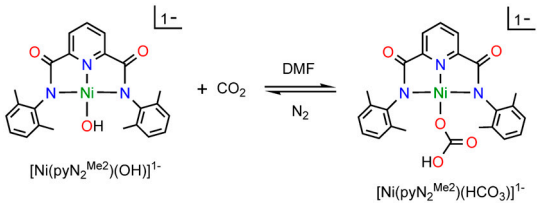

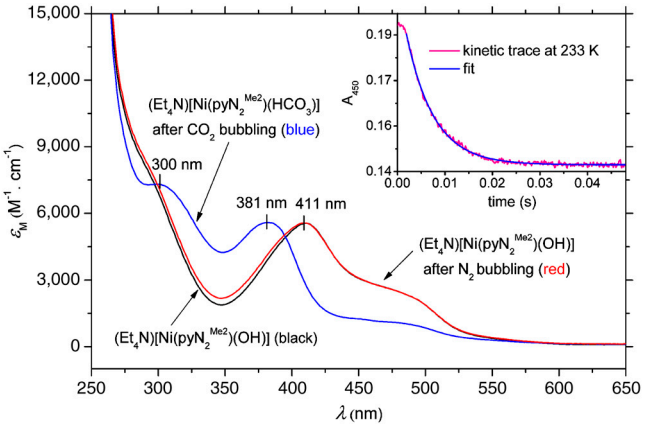

Fig. 1. Absorption spectra in DMF: black trace—$(Et_4N)[Ni(pyN_2^{Me2})(OH)]$; blue trace—after bubbling CO_2 through the solution for 2 min; red trace—after vigorous bubbling of N_2 through the solution of $(Et_4N)[Ni(pyN_2^{Me2})(HCO_3)]$ (blue trace) for 20 min. (*Inset*) Kinetics trace acquired at 450 nm and 233 K overlaid with a single exponential fit to $A = A_\infty + \Delta A \exp(-k_{obs}t)$, where A_∞ is the absorbance after complete reaction, $\Delta A = A_0 - A_\infty$, A_0 is the initial absorbance, and k_{obs} is the observed rate constant. Reactant concentrations: $\{[Ni(pyN_2^{Me2})(OH)]^{1-}\} = 0.1$ mM, $[CO_2] = 1$ mM.

Several features of the CO_2 fixation reaction 1 are noteworthy. The reactant is a terminal hydroxide species affording a unidentate bicarbonate (η^1-OCO_2H) product. Far more common is the reaction of bridged $M^{II}_2(\mu\text{-}OH)_{1,2}$ precursors to afford binuclear or occasional trinuclear products bridged by carbonate utilizing two or three oxygen atoms (4–9). A second feature is the apparently fast reaction rate, given that CO_2 comprises only 0.039 vol % of the atmosphere. Although fixation of atmospheric CO_2 by metal hydroxide species has been previously observed (4, 5, 7, 10), including with Ni^{II} (7, 11–13), no quantitation of reaction rates and analysis of reaction mechanism are available. The fixation of carbon dioxide, whereby this greenhouse gas is rendered in chemically combined forms, is of current environmental and biological interest. Fixation leads to utilization of the compound as a renewable carbon resource in the formation of useful organic compounds, ideally in catalytically efficient systems (14, 15). Atmospheric capture of CO_2 allows its sequestration by various methods including conversion to metal carbonates (16). In biology, the ubiquitous Zn(II) enzyme carbonic anhydrase catalyzes the reversible hydration reaction $CO_2 + H_2O \rightleftharpoons HCO_3^- + H^+$, which among other functions leads to the removal of CO_2 from tissues in the mammalian respiratory process. Given the fore-

Author contributions: D.H., S.C.L., and R.H.H. designed research; D.H., O.V.M., L.L.T., and S.C.L. performed research; S.C.L. and E.V.R.-A. analyzed data; and S.C.L., E.V.R.-A., and R.H.H. wrote the paper.

The authors declare no conflict of interest.

[1]To whom correspondence should be addressed. E-mail: holm@chemistry.harvard.edu.

This article contains supporting information online at www.pnas.org/lookup/suppl/doi:10.1073/pnas.1017430108/-/DCSupplemental.

Table 1. Observed rate constants as a function of water content in DMF

Water, equiv vs Ni^{II}	k_{obs}, s^{-1}
0	88.2
800	82.4
1600	72.6
3200	49.7

Kinetics traces at 450 nm and 218 K were fitted to the single exponential $A = A_\infty + \Delta A \exp(-kt)$ defined in Fig. 1. Concentration of reactants: $\{[Ni(pyN_2^{Me2})(OH)]^{1-}\} = 0.1$ mM, $[CO_2] = 1.0$ mM. Each k_{obs} is the average of eight runs.

going factors, we have determined the kinetics of reaction 1 and examined its mechanism with the aid of theoretical calculations.

Results and Discussion

Kinetics of CO_2 Fixation. The kinetics of reaction 1 were determined in dimethylformamide (DMF) solutions by stopped-flow spectrophotometry at 218–243 K. As seen in Fig. 1, the absorption spectrum of $[Ni(pyN_2^{Me2})(OH)]^{1-}$ contains a peak at 411 nm and a shoulder near 490 nm, whereas the product $[Ni(pyN_2^{Me2})(HCO_3)]^{1-}$ presents maxima at 300 and 381 nm. The reaction was followed by absorbance changes at 450 nm under conditions of variable and constant CO_2 concentrations (≥10-fold excess of CO_2 with respect to Ni). In treating the low-temperature absorbance data, no evidence of a preequilibrium was found. A typical single exponential fit of the data (233 K) in the presence of a 10-fold excess of CO_2 is included as an inset, from which the pseudo-first-order rate constant k_{obs} can be evaluated. The influence of water on the reaction rate was investigated under the conditions of Table 1. The possibility that CO_2 is hydrated by small amounts of water in DMF by the reaction $CO_2 + H_2O \rightleftharpoons HCO_3^- + H^+$ and that bicarbonate reacts with $[Ni(pyN_2^{Me2})(OH)]^{1-}$ to form a carbonate complex and water appears remote. This situation has been encountered in Cu^{II}/CO_2 systems in acetonitrile, resulting in formation of a dinuclear carbonato complex (8). There is no significant effect on k_{obs} up to a mol ratio $H_2O/Ni^{II} \approx 1600:1$. Further, the reaction product isolated is definitely a *monoanionic* bicarbonate complex (3). We conclude that our kinetics results are unaffected by the presence of small amounts of water.

Values of k_{obs} vary linearly with CO_2 concentration at constant Ni^{II} concentration, as shown for four temperatures in Fig. 2, establishing that the reaction is first-order in CO_2 concentration. The reaction is first-order in Ni^{II} as follows from the exponential shapes of the kinetics traces in the presence of excess CO_2. Also, values of k_{obs} determined from the kinetic traces do not depend

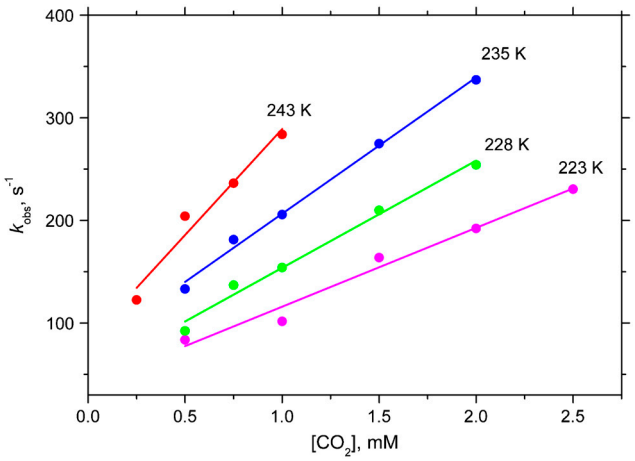

Fig. 2. Plots of the observed rate constants (k_{obs}) in DMF as a function of CO_2 concentration at 223–243 K and $\{[Ni(pyN_2^{Me2})(OH)]^{1-}\} = 0.1$ mM.

Table 2. Kinetics parameters for carbon dioxide fixation with $[Ni(pyN_2^{Me2})(OH)]^{1-}$ in DMF solutions

Experiment	$\Delta H^{\ddagger}$, kcal/mol	$\Delta S^{\ddagger}$, cal/mol K	k_2,* 228 K, $M^{-1}\,s^{-1}$	k_2,† 298 K, $M^{-1}\,s^{-1}$
Variable CO_2‡	4.7(1.5)	−15(5)	$1.04(7) \times 10^5$	—
Constant CO_2	3.2(5)	−20(3)	$1.45(1) \times 10^5$	9.5×10^5

*Experimental value.
†Extrapolated value.
‡See Fig. 2; k_2 at each temperature was determined from the slopes of k_{obs} vs $[CO_2]$ plots (data in *SI Text*).

on Ni^{II} concentration. Consequently, for reaction 1, rate $= k_2\{[Ni(pyN_2^{Me2})(OH)]^{1-}\}[CO_2]$. A full set of k_{obs} and k_2 data is available (*SI Text*). Second-order rate constants at 228 K and 298 K are given in Table 2 together with activation parameters obtained from the Eyring equation plotted in Fig. 3. The data plotted are from the experiment with constant $[CO_2] = 1$ mM. The negative activation entropies are consistent with an associative transition state.

Table 3 contains a summary of second-order rate constants for CO_2 fixation at ambient temperature, which may be compared with the extrapolated value of $k_2 = 9.5 \times 10^5$ $M^{-1}\,s^{-1}$ at 298 K for reaction 1. These data were obtained in aqueous solution in a pH range sufficient to deprotonate coordinated water and thus refer to the minimal reaction $M\text{-}OH + CO_2 \rightarrow M\text{-}OCO_2H$. The synthetic reactants $[L_nM\text{-}OH]^{z+}$ are primarily octahedral complexes of Co^{III} and five-coordinate $[Zn(cyclen)(OH)]^{1+}$, perhaps the most successful kinetics mimic of the carbonic anhydrase site (17). Of the multitude of kinetics information available for carbonic anhydrase, data for the human enzymes I, II, and III are selected because of the availability of k_{cat} and K_M data. It is evident that the rate constant for reaction 1 enters the domain of carbonic anhydrase kinetics and is $\gtrsim 10^2$ faster than any metal-mediated synthetic system executing the same reaction. Although a more exact comparison cannot be made because of differences in solvent, this reaction is by any standard an extremely rapid CO_2 fixation. Like most other fixation reactions that have been adequately described, reaction 1 is reversible. Purging a solution of preisolated $[Ni(pyN_2^{Me2})(HCO_3)]^{1-}$ with dinitrogen results in quantitative recovery of $[Ni(pyN_2^{Me2})(OH)]^{1-}$ (Fig. 1).

Reaction Mechanism. The mechanism of reaction 1 was investigated by density functional theory (DFT) calculations. For comparison and calibration, different combinations of functionals (BP86, B3LYP) and basis sets [6-31G(d), DGDZVP] were em-

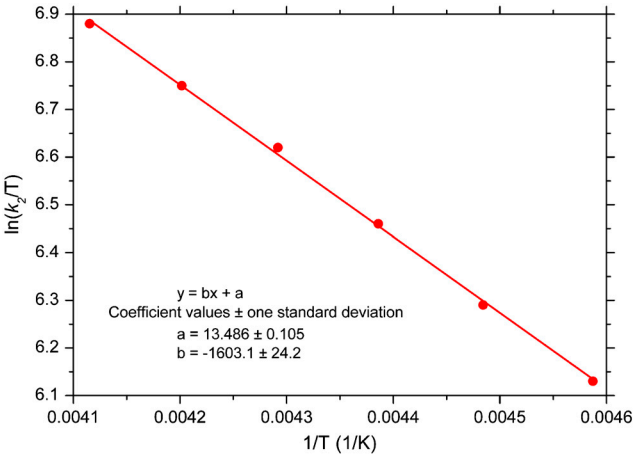

Fig. 3. Eyring plot for the reaction of 0.1 mM $[Ni(pyN_2^{Me2})(OH)]^{1-}$ with 1 mM CO_2 in DMF. The data were analyzed with the equation $k_2 = [(k_BT)/h]\exp(-\Delta G^{\ddagger}/RT)$ with $\Delta G^{\ddagger} = \Delta H^{\ddagger} - T\Delta S^{\ddagger}$. Activation parameters are given in Table 2.

Table 3. Comparative rate constants for the reaction of CO_2 and M-OH groups

Reactant	k_2 or k_{cat}/K_M, $M^{-1}\,s^{-1}$*	Ref.
$[L_nM^{III}\text{-}OH]^{z+}$	41–590	(18†–20)
$[Zn(cyclen)(OH)]^{1+}$	3.3×10^3	(17)
OH^-	7.9×10^3	(21)
Human carbonic anhydrase‡	1.1×10^5 to 1.6×10^8	(17)

*Aqueous solution, pH ~ 7–9 (where specified).
†See additional data and references cited therein.
‡k_{cat}/K_M.

ployed on the full pyN_2^{Me2} systems as well as on simpler N-H and N-Me complexes. Calculations were conducted in the gas phase, where the monoanionic complexes were found to be stable to electron autodetachment (negative highest occupied molecular orbital and positive vertical ionization energies), and also with use of a polarizable continuum solvent model to simulate the experimental DMF solvent medium. In general, the various approaches all gave the same qualitative description of the reaction pathway; attention is focused on the pyN_2^{Me2} complexes. The BP86/6-31G(d) enthalpic reaction profile and stationary point geometries are provided in Fig. 4, and a schematic reaction sequence of the reactive fragments showing relative orientations and bond distances is given in Scheme 1. Calculated enthalpies with different computational models are listed in Table 4.

The computed reaction begins with formation of a weakly associated precursor complex (PC) from the reactants at infinite separation. The CO_2 molecule approaches along the approximate mirror plane perpendicular to the NiN_3 plane between the faces of the $C_6H_3Me_2$ (DMP) substituents. With the exception of transition states involving nickel–bicarbonate rotation, all subsequent CO_2-derived fragments lie on this plane. The closest contact between reactants in the PC occurs between the hydroxyl oxygen O1 and the CO_2 carbon atom at a distance shorter than the van der Waals separation (2.5–3.0 Å, depending on the method and basis set) (22). The interaction is limited, however, as the CO_2 molecule deviates little from linearity (170–177°). Although PC formation is enthalpically favorable, the loss in entropy probably renders the complex slightly higher in free energy than the separated reactants at the experimental temperatures; this, plus the limitations of DFT treatments of weak interactions, limits the experimental significance of the precursor complex.

From PC, the reaction proceeds through a four-centered transition state (TS_{ins}) that inserts an O-C fragment into the Ni-OH bond. Conceptually, this transition state represents a nucleophilic attack of metal-bound hydroxide (O1H) at electrophilic carbon atom, with concurrent formation of a new Ni-O interaction from one of the CO_2 oxygen atoms (O2). This transition state closely resembles that accepted for CO_2 fixation by carbonic anhydrase (23, 24), albeit with a different metal, d-electron count, and stereochemistry. For BP86 calculations, the wave function at the transition state is stable as a spin-restricted singlet. In contrast, stability tests on B3LYP calculations reveal lower energy, unrestricted solutions. The energy differences between the geometry-optimized unrestricted and restricted wave functions are minor (<1.5 kcal/mol), however, and the corresponding structures deviate by <0.08 Å in Ni-ligand distances. An alternative reaction pathway was also characterized, involving a transition state (TS_{pt}) with simultaneous proton transfer and O1-C bond formation. This route does not involve direct Ni-CO_2 interaction, and O1 remains bound to the Ni center from reactant to product. The calculated activation enthalpy for TS_{pt}, however, is at least 12 kcal/mol higher than that of TS_{ins} across all calculations, and this pathway therefore appears irrelevant to the mechanism of reaction 1.

The immediate product from TS_{ins} is the nickel–bicarbonate complex P1, with the bicarbonate ligand adopting an antiperiplanar orientation of the Ni—O2—C=O3 dihedral and a synperiplanar O3=C—O1—H dihedral. This product geometry can rear-

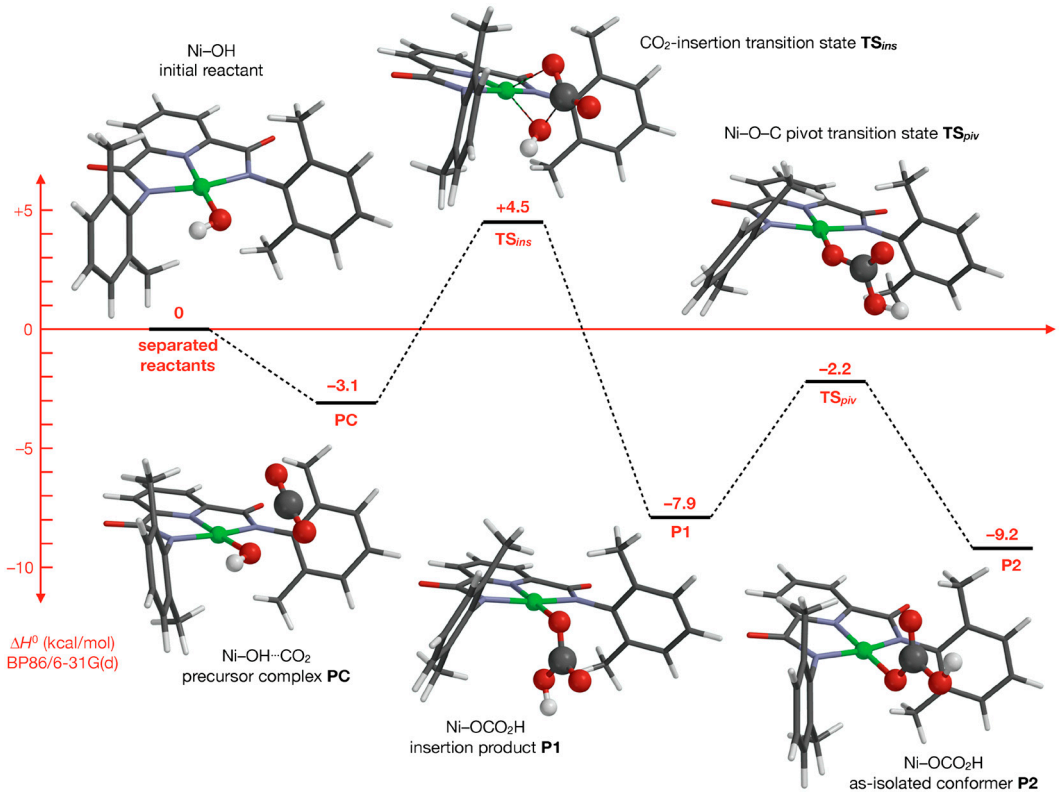

Fig. 4. BP86/6-31G(d) reaction profile and stationary point structures for CO_2 fixation by $[Ni(pyN_2^{Me2})(OH)]^{1-}$. Energy values (kcal/mol) are standard enthalpies of reaction or activation.

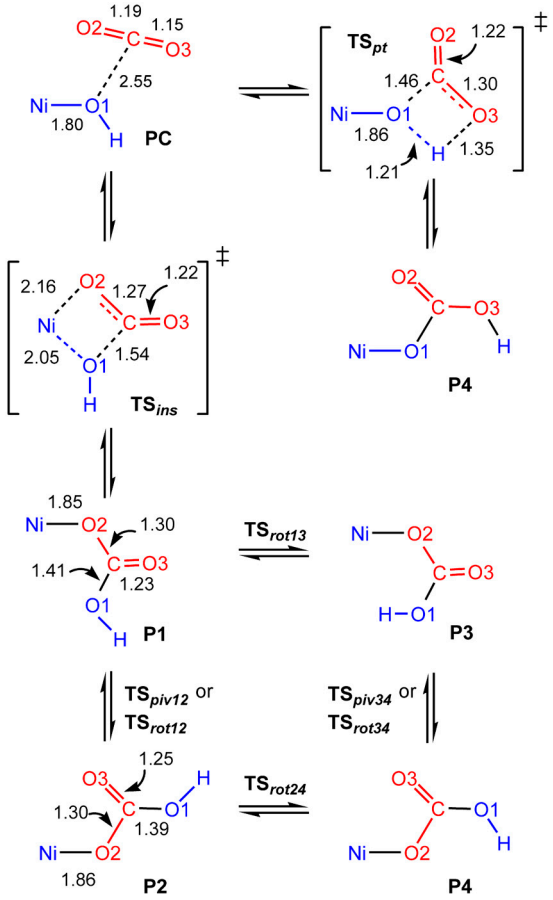

Scheme 1. Summary of the events in Fig. 4 with computed bond lengths (Å) from BP86/6-31G(d) optimizations for species along the reaction profile of Fig. 4. Note that TS_{pt} and P4 are not involved in the reaction scheme (see text).

range to the more stable synperiplanar Ni—O2—C═O3 conformation P2 by pivoting about the O2 linkage through transition state TS_{piv12}; this trajectory is equivalent to simultaneous rotations about both the Ni—O2 and O2—C bonds. Direct rotation by 180° about the O2—C bond offers a simpler, alternative reorientation pathway; our calculations indicate that this route is less favorable energetically by >2.4 kcal/mol (TS_{rot12}). Further rotations about the Ni—O1 bond in P1 and P2 through transition states TS_{rot13} and TS_{rot24} lead to antiperiplanar O3═C—O1—H conformers P3 and P4, respectively. These can be interconverted directly by O2 pivot or O2—C rotation pathways analogous to those linking P1 and P2 with the barrier to rotation (TS_{rot34}) lower than the pivot barrier (TS_{piv34}) in this case. Of the bicarbonate orientations, the most stable are the nearly equienergetic P2 and P4 conformers. P2 corresponds to the crystallographic product structure (3), although this structure also possesses additional interactions due to hydrogen-bonded dimerization via the bicarbonate ligand. This hydrogen bonding, which is not possible for the antiperiplanar O3═C—O1—H orientation of P4, probably determines the P2 geometry in the crystal structure, and similar interactions, either via self-association or, more likely, with the DMF solvent, may also favor P2 in solution.

The computational results agree well with available experimental findings. Structurally, the calculated geometries of $[Ni(pyN_2^{Me2})(OH)]^{1-}$ and the P2 conformer can be tested against crystallographic determinations (3) (*SI Text*). The Ni-ligand distances are within the expected accuracies in all DFT approaches investigated, and there is little basis to favor any particular computational model in our comparison set. The ligand conformations are predicted correctly, with the hydroxide hydrogen atom lying in the Ni coordination plane and the DMP substituents canted toward each other on one side of the coordination plane. Ignoring the hydroxide proton, the coordination unit and N-substituents assumes approximate C_s symmetry. A different conformer with the same in-plane hydroxide orientation, but with DMP groups canted in a parallel manner (approximate C_2 symmetry), was also identified computationally at essentially the same energy. Because the CO_2 insertion occurs via the C_s orientation, this geometry was used for the reactant reference energy in all thermochemical comparisons. For P2, distances within the bicarbonate ligand deviate significantly from the experimental data, due presumably to hydrogen bonding in the solid state structure.

Energetically, the calculated activation enthalpies agree well with and bracket the values obtained from reaction kinetics (Tables 2 and 4), with the BP86 and B3LYP results higher and lower, respectively, than experiment. The magnitudes of the entropies are unreliable, being consistently higher than experiment by *ca.* 14–17 cal/mol K; at the computed entropies, the overall thermochemistry of reaction 1 at 298.15 K from infinite separation to the bicarbonate product is incorrectly predicted to be either endergonic (BP86) or so weakly exergonic (≤ -5 kcal/mol, B3LYP) that a substantial dissociative equilibrium arises.

Table 4. Computed standard enthalpies (kcal/mol) and entropies (in parentheses, cal mol^{-1} K^{-1}) for stationary points on reaction 1 pathway*

Method/basis set	PC	TS_{ins}	TS_{pt}	P1†	TS_{piv12}	TS_{rot12}	P2†	TS_{rot13}	P3	TS_{rot24}	P4†	TS_{piv34}	TS_{rot34}
B3LYP/6-31G(d)	−5.1	0.6‡	17.7	−12.9	−7.3	−4.6	−14.6	−4.7	−9.1	−6.5	−14.9	−5.7	−6.7
	(−24)	(−34)	(−30)	(−31)	(−37)	(−39)	(−32)	(−35)	(−32)	(−32)	(−33)	(−35)	(−38)
(DMF solvation)	−1.7	0.2‡	17.8	−13.5	−7.5‡	−5.1‡	−14.6	−5.6	−11.4	−6.2	−14.3	−6.9‡	−7.9‡
	(−24)	(−34)	(−32)	(−34)	(−37)	(−39)	(−34)	(−35)	(−34)	(−35)	(−33)	(−34)	(−38)
B3LYP/DGDZVP	−4.4	2.6‡	18.2	−11.9	−6.5	−3.6†	−13.1	−4.0	−8.3	−5.4	−13.4	−4.9	−5.9
	(−26)	(−35)	(−29)	(−36)	(−38)	(−37)	(−34)	(−37)	(−32)	(−34)	(−33)	(−36)	(−39)
(DMF solvation)	0.1	1.9‡	18.7	−11.9	−6.7	−3.6	−12.3	−4.4	−10.3	−4.6	−12.3	−6.4	−6.5
	(−25)	(−34)	(−35)	(−33)	(−36)	(−41)	(−36)	(−38)	(−35)	(−37)	(−37)	(−36)	(−42)
BP86/6-31G(d)	−3.1	4.5	18.4	−7.9	−2.2	1.3	−9.2	−0.3	−6.0	−1.4	−9.6	−1.1	−1.6
	(−26)	(−36)	(−34)	(−34)	(−38)	(−40)	(−35)	(−35)	(−34)	(−34)	(−35)	(−38)	(−41)
(DMF solvation)	−0.2	4.6	18.7	−8.8	−2.2	0.7	−9.6	−1.2	−7.9	−1.5	−9.4	−1.7	−2.3
	(−27)	(−35)	(−38)	(−36)	(−37)	(−41)	(−35)	(−37)	(−33)	(−35)	(−34)	(−35)	(−41)
BP86/DGDZVP	−2.5	5.3	17.4	−8.2	−2.7	0.8	−9.0	−1.1	−6.7†	−1.8	−9.3	−1.7	−2.2
	(−24)	(−37)	(−31)	(−36)	(−37)	(−38)	(−35)	(−36)	(−34)	(−33)	(−33)	(−38)	(−39)
(DMF solvation)	1.0	5.1	17.7	−8.7	−3.0	0.5	−8.9	−1.7	−8.4†	−1.4	−9.0	−2.9	−2.9
	(−25)	(−35)	(−35)	(−36)	(−39)	(−41)	(−38)	(−39)	(−36)	(−39)	(−38)	(−38)	(−42)

*Structures are C_1 symmetric unless otherwise indicated.
†C_s symmetric.
‡Unrestricted singlet calculation due to wave function instability.

The erroneous entropies can be attributed to the inaccurate computational description of low-frequency vibrational modes (25). If the experimental activation entropy (-20 cal/mol K, giving $T\Delta S = +6$ kcal/mol at 298.15 K) is applied, consistently exergonic reactions are obtained. With this assumption and using the largest computed free energies of reaction [B3LYP/6-31G(d)], a solution of P2 at 1-mM initial concentration contains a low but nonneglible concentration (*ca.* 0.01–0.02 mM) of the hydroxide complex at equilibrium. This concentration was obtained using speciation equilibria involving $[Ni(pyN_2^{Me2})(OH)]^{1-}$, CO_2, and products P1–P4; the formation of PC is probably endergonic and was therefore excluded in the calculation. The result is consistent with the observed reversal of reaction 1 by dinitrogen sparging (Fig. 1).

From the computational results, we make the following observations: (*i*) the planar Ni^{II} geometry provides an unhindered, out-of-plane approach for the small CO_2 reactant; (*ii*) the insertion process involves the simultaneous formation of new C···O1 and Ni···O2 interactions that compensate for the reduction of bonding character from the initial unperturbed Ni—O1 and C═O2 moieties; and (*iii*) aside from the local geometry changes associated with substrate insertion, the nickel complex is otherwise unchanged over the course of the reaction. The confluence of these factors likely accounts for the exceedingly low activation for CO_2 insertion. Finally, we note that our computational models do not address hydrogen bonding, and, given the low energies involved in this system, these interactions may be contributors to the overall solution thermochemistry.

Materials and Methods

Kinetics Measurement. Commercial DMF was dried over 3-Å molecular sieves for 3 d, redistilled in vacuo from CaH_2 at 55 °C, and degassed by purging with dinitrogen gas before use in the glove box. Solutions of $(Et_4N)[Ni(pyN_2^{Me2})(OH)]$ (3) were prepared in a glove box filled with argon immediately before a kinetics run and manipulated with a Hamilton gastight syringe equipped with a three-way valve. The solubility of CO_2 in DMF has been reported as 0.18 M (26) and 0.20 M (27, 28); the latter value was used. Saturated solutions were prepared by bubbling CO_2 through argon-saturated DMF in a syringe at 298 K for 20 min. Solutions with lower CO_2 concentrations were prepared by multiple dilutions of a 0.20-M solution with argon-saturated DMF using graduated gastight syringes equipped with three-way valves; liquid phase occupied the entire available volume in the closed system and was never exposed to the atmosphere and/or the gas/vapor phase. Kinetics measurements were performed on a Hi-Tech Scientific SF-43 multimixing anaerobic cryogenic stopped-flow instrument (mixing time 4 ms) using a visible lamp. Because the reactions are very fast, data were collected in a single wavelength mode. All measurements were performed at 450 nm (the visible lamp afforded noisy spectra of $[Ni(pyN_2^{Me2})(OH)]^{1-}$ at $\lambda_{max} = 411$ nm). Solutions of the Ni^{II} complex and CO_2 in DMF were separately cooled at low temperature (218–243 K) and mixed in a 1:1 volume ratio. The mixing cell temperature was maintained at ± 0.1 K. Concentrations of all reagents are reported for the onset of the reaction (after mixing). CO_2 (0.25–2.5 mM) was always in excess with respect to $[Ni(pyN_2^{Me2})(OH)]^{1-}$ (0.1 mM). Data analysis was performed with Rapid Kinetics software (Hi-Tech Scientific) and confirmed by IgorPro program for kinetics traces at 450 nm using a single exponential fit. Each reported rate constant is an average of at least five runs with standard deviations within $\pm 2\%$.

Computational Methods. Density functional calculations were performed using the Gaussian 09 (G09) software package (29). B3LYP (30–32) and BP86 (30, 33) functionals were employed in combination with split valence double-zeta, singly polarized 6-31G(d) (34, 35) and DGDZVP (36, 37) basis sets. Stationary points (minima or transition states) were verified by frequency calculations, and reaction paths from transition states were identified by tracking intrinsic reaction coordinates (38, 39). Solvation effects were investigated via the polarizable continuum model using the integral equation formalism (40), which is the default self-consistent reaction field method in G09. Initial geometry optimizations were conducted on restricted singlet states, and all converged wave functions were tested for stability (41, 42); unstable wave functions were reoptimized to stable unrestricted wave functions that were then subjected to further geometry optimization and wave function stability analyses. Default convergence criteria and parameters were used throughout.

ACKNOWLEDGMENTS. This research was supported at Harvard University by the National Institutes of Health (GM-28856), at Tufts University by the National Science Foundation (Chemistry Grant 0750140 and Chemistry Research, Instrumentation, and Facilities Grant 0639138), and at the University of Waterloo by the Natural Sciences and Engineering Research Council, Canada Foundation for Innovation, Ontario Research Fund, and the Shared Hierarchical Academic Research Computer Network.

1. Jeoung J-H, Dobbek H (2007) Carbon dioxide activation at the Ni,Fe-cluster of anaerobic carbon monoxide dehydrogenase. *Science* 318:1461–1464.
2. Kung Y, Doukov TI, Seravalli J, Ragsdale SW, Drennan CL (2009) Crystallographic snapshots of cyanide- and water-bound C-clusters from bifunctional carbon monoxide dehydrogenase/acetyl-CoA synthase. *Biochemistry* 48:7432–7440.
3. Huang D, Holm RH (2010) Reactions of the terminal Ni^{II}-OH group in substitution and electrophilic reactions with carbon dioxide and other substrates: structural definition of binding modes in an intramolecular Ni^{II}…Fe^{II} bridged site. *J Am Chem Soc* 132:4693–4701.
4. Kitajima N, Fujisawa K, Koda T, Hikichi S, Moro-oka Y (1990) Fixation of atmospheric CO_2 by a copper(II) Complex. *Chem Commun* 1357–1358.
5. Murthy NN, Karlin KD (1993) A dinuclear zinc hydroxide complex which traps atmospheric carbon dioxide: formation of a tri-zinc complex with a triply bridging carbonate group. *Chem Commun* 1236–1238.
6. Looney A, Han R, McNeill K, Parkin G (1993) Tris(pyrazolyl)hydroboratozinc hydroxide complexes as functional models for carbonic anhydrase: on the nature of the bicarbonate intermediate. *J Am Chem Soc* 115:4690–4697.
7. Kitajima N, Hikuchi S, Tanaka M, Moro-oka Y (1993) Fixation of atmospheric CO_2 by a series of hydroxo complexes of divalent metal ions and the implication for the catalytic role of metal ion in carbonic anhydrase Synthesis, characterization, and molecular structure of $[LM(OH)]_n$ ($n = 1$ or 2) and $LM(\mu\text{-}CO_3)ML$ (M(II) = Mn, Fe, Co, Ni, Cu, Zn; L = HB(3,5-*i* Pr_2 *pz*)$_3$). *J Am Chem Soc* 115:5496–5508.
8. Company A, et al. (2007) Structural and kinetic study of reversible CO_2 fixation by dicopper macrocyclic complexes. From intramolecular binding to self-assembly of molecular boxes. *Inorg Chem* 46:9098–9110.
9. Bergquist C, Fillebeen T, Morlok MM, Parkin G (2003) Protonation and reactivity towards carbon dioxide of the mononuclear tetrahedral zinc and cobalt hydroxide complexes, $[Tp^{Bu^t,Me}]ZnOH$ and $[Tp^{Bu^t,Me}]CoOH$: Comparison of the reactivity of the metal hydroxide function in synthetic analogues of carbonic anhydrase. *J Am Chem Soc* 125:6189–6199.
10. Bazzicalupi C, et al. (1996) CO_2 fixation by novel copper(II) and zinc(II) macrocyclic complexes. A solution and solid state study. *Inorg Chem* 35:5540–5548.
11. Ito M, Takita Y (1996) Atmospheric CO_2 fixation by dinuclear Ni(II) complex, $[TPANi(II)(\mu\text{-}OH)_2TPA](ClO_4)_2$ (TPA = tris(pyridylmethyl)amine). *Chem Lett* 929–930.
12. Kersting B (2001) Carbon dioxide fixation by binuclear complexes with hydrophobic binding pockets. *Angew Chem Int Edit* 40:3987–3990.
13. Wikstron JP, et al. (2010) Carbonate formation within a nickel dimer: Synthesis of coordinatively unsaturated bis(μ-hydroxo) dinickel complex and its reactivity toward carbon monoxide. *Dalton Trans* 39:2504–2514.
14. Sakahura T, Choi J-C, Yasuda H (2007) Transformation of carbon dioxide. *Chem Rev* 107:2365–2387.
15. He L-N, Wang J-Q, Wang J-L (2009) Carbon dioxide chemistry: Examples and challenges in chemical utilization of carbon dioxide. *Pure Appl Chem* 81:2069–2080.
16. Lackner KS (2003) A guide to CO_2 sequestration. *Science* 300:1677–1678.
17. Zhang X, van Eldik R (1995) A functional model for carbonic anhydrase: Thermodynamic and kinetic study of a tetraazacyclodecane complex of zinc(II). *Inorg Chem* 34:5606–5614.
18. Palmer DA, van Eldik R (1983) The chemistry of metal carbonate and carbon dioxide complexes. *Chem Rev* 83:651–731.
19. Acharya AN, Dash AC (1993) Kinetics of the reversible uptake of carbon dioxide and sulphur dioxide by the *cis*-(Hydroxo)(imidazole)*bis*(ethylenediamine)-cobalt(III) ions in aqueous medium. A comparative study. *Proc Indian Acad Sci (Chem Sci)* 105:225–233.
20. Jacewicz D, Chylewska A, Daakbrowska A, Chmurzynski L (2007) Stopped-flow spectrophotometric study on the reaction between carbon dioxide and $[Co(NH_3)_4(H_2O)_2]^{3+}$ ion in aqueous solution. *Z Anorg Allg Chem* 633:1493–1499.
21. Zhang X, van Eldik R, Koike T, Kimura E (1993) Kinetics and mechanism of the hydration of CO_2 and dehydration of HCO_3^- catalyzed by a Zn(II) complex of 1,5,9-triazacyclododecane as a model for carbonic anhydrase. *Inorg Chem* 32:5749–5755.
22. Rowland RS, Taylor R (1996) Intermolecular nonbonded contact distances in organic crystal structures: Comparison with distances expected from van der Waals radii. *J Phys Chem* 100:7384–7391.
23. Lindskog S, Liljas A (1993) Carbonic anhydrase and the role of orientation in catalysis. *Curr Opin Struct Biol* 3:915–920.
24. Christianson DW, Fierke CA (1996) Carbonic anhydrase: Evolution of the zinc binding site by nature and by design. *Acc Chem Res* 29:331–339.
25. Cramer CJ (2004) *Essentials of Computational Chemistry* (Wiley, Chichester, UK).
26. Pocker Y, Bjorkquist DW (1977) Comparative studies of bovine carbonic anhydrase in H_2O and D_2O. Stopped flow studies of the kinetics of interconversion of CO_2 and HCO_3^-. *Biochemistry* 16:5698–5707.
27. Gennaro A, Isse AA, Vianello E (1990) Solubility and electrochemical determination of CO_2 in some dipolar aprotic solvents. *J Electroanal Chem* 289:203–215.

28. Tezuka M, Iwasaki M (1993) Voltammetric study on CO_2 reduction electrocatalyzed by cobalt tetraphenylporphine in DMF solution. *Chem Lett* 427–430.
29. Frisch MJ, et al. (2009) Gaussian 09, Revision A.02. (Gaussian Inc, Wallingford, CT).
30. Becke AD (1988) Density-functional exhange-energy approximation with correct asymptotic behavior. *Phys Rev A* 38:3098–3100.
31. Lee C, Yang W, Parr RG (1988) Development of the colle-salvetti correlation-energy formula into a functional of the electron density. *Phys Rev B* 37:785–789.
32. Miehlich B, Savin A, Stoll H, Preuss H (1989) Results obtained with the correlation-energy density functionals of Becke and Lee, Young and Parr. *Chem Phys Lett* 157:200–206.
33. Perdew JP (1986) Density-functional approximation for the correlation energy of the inhomogeneous electron gas. *Phys Rev B* 33:8822–8824.
34. Rassolov VA, Pople JA, Ratner MA, Windus TL (1998) 6-31G* basis set for atoms K through Zn. *J Chem Phys* 109:1223–1229.
35. Rassolov VA, Ratner MA, Pople JA, Redfern JA, Curtiss LA (2001) Basos set for third-row atoms. *J Comput Chem* 22:976–984.
36. Godbout N, Salahub DR, Andzelm J, Wimmer E (1992) Optimatization of Gaussian-type basis sets for local spin density functional calculations. Part I. Boron through neon, optimization technique and validation. *Can J Chem* 70:560–571.
37. Sosa C, et al. (1992) A local density functional study of the structure and vibrational frequencies of molecular transition metal compounds. *J Phys Chem* 96:6630–6636.
38. Hratchian HP, Schlegel HB (2004) Accurate reaction paths using a Hessian-based predictor-corrector integrator. *J Chem Phys* 120:9918–9924.
39. Hratchian HP, Schlegel HB (2005) Using Hessian updating to increase the efficiency of a Hessian-based predictor-corrector reaction pathway following method. *J Chem Theory Comput* 1:61–69.
40. Tomasi J, Mennucci B, Cammi R (2005) Quantum mechanical continuum solvation models. *Chem Rev* 105:2999–3093.
41. Seeger R, Pople JA (1977) Self-consistent molecular orbital methods. XVIII. Constraints and stability in Hartree-Fock theory. *J Chem Phys* 66:3045–3050.
42. Bauernschmitt R, Ahlrichs R (1996) Stability analysis for solutions of the closed shell Kohn-Sham equation. *J Chem Phys* 104:9047–9052.